International Journal of
AI ELECTRICAL CIVIL AND MECHANICAL ENGINEERING
Peer Reviewed, Referred & Indexed Journal
ISSN: 3070-0434 www.zesterapublications.com Original Research Paper

Uncertainty-Aware Geostatistical Reconstruction of Regional Groundwater Hydraulics under Sparse Monitoring Conditions: A Case Study of the Evergreen Underground Water Conservation District (EUWCD), Texas, USA

Mir Akib Jawed

MSc in Water Resource Science and Technology
Texas A&M University-San Antonio, Texas

Abstract

Adequate estimation of hydraulic head fields in regional aquifers is critical for sustainable groundwater management, but in rural aquifers monitoring networks are often sparse, uneven, and temporally irregular, leading to large and poorly quantified interpolation uncertainty. This study proposes and tests an uncertainty-aware geostatistical approach to reconstruct the regional potentiometric surface of the Carrizo–Wilcox aquifer under the Evergreen Underground Water Conservation District (EUWCD) in South-Central Texas. A total of 180 monitoring wells provided 4,872 hydraulic head observations from 2005 to 2022 that were analyzed. The following six spatial predictors were contrasted: ordinary kriging (OK), universal kriging (UK), kriging with external drift (KED) (with land-surface elevation as the external drift variable), Bayesian kriging (BK), sequential Gaussian simulation (SGSIM) (with 500 realizations), and a combination of Random Forest and krigged residuals (RFK). Leave-one-out cross-validation and independent hold-out testing (22 wells) were used to evaluate model performance, whilst predictive uncertainty was evaluated using kriging variance, Bayesian posterior variance, and ensemble standard deviation. The omnidirectional spatial structure was best represented by a spherical variogram with a nugget of 18 m2, a partial sill of 105 m2 and a range of 22 km, while a moderate geometric anisotropy (ratio 1.44) was found, consistent with the regional dip. RFK produced the lowest overall error (RMSE = 2.68 m, $R^2 = 0.934$), followed by KED (RMSE = 2.91 m). SGSIM realizations reproduced the observed head statistics while providing spatially explicit uncertainty maps; the mean ensemble standard deviation was 4.7 m across the domain but exceeded 8.5 m in downdip sub-regions with < 0.15 wells km^{-2}. Based on a sensitivity analysis of well density and the resulting uncertainty in prediction, the well density range of 0.6–1.0 wells km^{-2} was determined to be an efficient design envelope. The framework offers EUWCDs and similar rural water-management entities a clear, defensible and replicable process for regional groundwater characterization and prioritization of monitoring investments.

Keywords—*Geostatistics, hydraulic head, kriging, sequential Gaussian simulation, Bayesian, Random Forest, uncertainty quantification, Carrizo–Wilcox aquifer, Texas, sparse monitoring.*

I. Introduction

In many semi-arid and drought-prone areas of the United States, groundwater is the source of water for municipal, industrial, and agricultural use [1]. Groundwater supplies about 55 % of the water used in Texas, and the Carrizo–Wilcox aquifer is the second largest source in the state, after the Ogallala [2]. The Carrizo–Wilcox is a multi-layered, semi-confined to confined, sandstone system that stretches from the Rio Grande to the Louisiana border, with the middle- and lower-Wilcox strata serving as the main source for many underground water conservation districts (GCDs) in South-Central Texas [3]. Over the last two decades, the Interstate-35 corridor has seen a sustained population growth, an increased demand for water from the oil-field development of the Eagle Ford Shale, and frequent multi-year droughts, all of which have added unprecedented strain to this aquifer [4]. Thus, good science-based management requires good, spatially explicit, and uncertainty-quantified reconstructions of the regional potentiometric surface.

International Journal of
AI ELECTRICAL CIVIL AND MECHANICAL ENGINEERING
Peer Reviewed, Referred & Indexed Journal
ISSN: 3070-0434 www.zesterapublications.com Original Research Paper

Spatial interpolation is an inherent problem in reconstructing regional groundwater hydraulics from point observations. Geostatistics has been the major paradigm that has been adopted to solve these problems since Matheron's early work and the development of the theory of regionalized variables in hydrogeology [5, 6]. Ordinary kriging (OK), universal kriging (UK) and kriging with external drift (KED) are not only best-linear-unbiased estimators but also provide an explicit expression for the estimation variance, which can be used to provide a first-order characterization of the predictive uncertainty [7]. The Bayesian versions of kriging (BK) further develop this idea by introducing randomness in the variogram parameters, which is then propagated into the posterior distributions of the estimate [8]. Sequential Gaussian simulation (SGSIM) generates Monte Carlo realizations in such a way that both the variogram and the conditioning data are respected, giving a spatially non-smoothed picture of the uncertainty which is important if the simulated field is used as an input to flow or transport models [9], [10].

The combination of geostatistics and machine-learning algorithms has been explored in more recent literature. Regression kriging and hybrid methods (like Random Forest with kriged residuals (RFK)) provide a way to fuse the flexibility of non-parametric learners in modeling the deterministic component (drift) that is caused by auxiliary variables (topography, geology, distance to features) and the stochastic strengths of kriging in modeling the residual spatial correlation [11] [12]. A similar Bayesian machine-learning approach, Gaussian process regression, has also become popular in groundwater applications, especially in data-poor settings [13]. Comparative studies indicate that there is no unique best method, but the performance depends on the density of the data, the magnitude of the deterministic drift, spatial anisotropy and the type of objective, whether deterministic prediction or ensemble uncertainty [14, 15].

Even with these methodological improvements, one of the challenges for rural areas, such as the aquifers of South and Central Texas and much of the western United States, is the sparsity and irregularity of observation networks. Well densities in many GCDs are below 1 well per 5 km², monitoring well sampling is often limited to once a year or twice, and monitoring wells are often placed along roads or property lines instead of along optimal geostatistical designs [16], [17]. This means that there are significant uncertainties in the estimated potentiometric surfaces that are not well documented, which compromises permitting, drought triggers, and regional water planning. Previous geostatistical analysis of Texas aquifers has mainly involved deterministic reconstruction [18, 19] or transmissivity mapping [20] and few have explored multiple approaches, systematically quantified spatial uncertainty and incorporated such uncertainty into monitoring design in a GCD-specific context.

This study fills that void for the Evergreen Underground Water Conservation District (EUWCD), a four-county conservation district (Atascosa, Frio, Karnes, and Wilson) in South-Central Texas overlying the Carrizo–Wilcox aquifer and experiencing increasing demand from municipal, agricultural, and oil-and-gas users. The specific objectives are: (i) to develop a rigorous geostatistical characterization of the regional hydraulic head field from a quality-controlled multi-decadal dataset of 4,872 observations from 180 monitoring wells; (ii) to compare the predictive accuracy and uncertainty characterization of six methods (OK, UK, KED, BK, SGSIM, and RFK) using leave-one-out cross-validation and a spatially stratified hold-out sample; (iii) to quantify the sensitivity of predictive uncertainty to observation-network density and to identify an efficient monitoring design envelope; and (iv) to translate the findings into actionable recommendations for EUWCD and analogous rural GCDs. The integrated framework is designed to transition from deterministic head mapping to defensible, uncertainty-explicit hydrogeological characterization that can be used to manage the system adaptively in the face of climate and demand nonstationarity.

International Journal of
AI ELECTRICAL CIVIL AND MECHANICAL ENGINEERING
Peer Reviewed, Referred & Indexed Journal
ISSN: 3070-0434 www.zesterapublications.com Original Research Paper

II. Study Area

The Evergreen Underground Water Conservation District covers approximately 12,140 km² across Atascosa, Frio, Karnes, and Wilson counties in South-Central Texas. The Guadalupe River basin is to the north and the Nueces River basin to the south. The topography of the region is subdued, and slopes gently from northwest to southeast with land-surface elevations of approximately 220 m above mean sea level (amsl) near the Balcones Escarpment and less than 60 m amsl along the southeastern edge of the district. Climate is subtropical, subhumid to semi-arid, with mean annual precipitation ranging from 620 mm (west) to 830 mm (east), with the majority of the precipitation occurring in spring and early autumn, and potential evapotranspiration is greater than precipitation during each month [21].

The principal groundwater resource is the Carrizo–Wilcox aquifer, a multi-layer, Paleocene–Eocene age, sandstone system. The aquifer sequence is gently dipping to the southeast at about 1.5° and consists of the Hooper Shale (lower confining member), the Simsboro Sand (middle Wilcox), the Calvert Bluff Shale (upper Wilcox), and the overlying Carrizo Sand. The total saturated thickness in EUWCD varies from approximately 90 m at the updip outcrop to more than 350 m in the downdip subsurface. Transmissivity ranges from < 100 m² d⁻1 in the fine-grained facies in the downdip to > 900 m² d⁻1 near the outcrop in the Simsboro Sand [22]. Recharge is primarily along the Carrizo and Wilcox outcrop belt that traverses the northwestern part of the district and secondarily by leakage from overlying formations and faults that are part of the Wilcox Growth Fault Zone (Fig. 1).

The land use is primarily rangeland (46 %), cropland (28 %) and pasture (16 %), with urban development increasing around Pleasanton, Jourdanton and Kenedy. Groundwater supplies are used for virtually 100 % of rural domestic supply and about 62 % of municipal supply. The Eagle Ford Shale oil and gas play has introduced a major new demand vector for water for drilling and hydraulic fracturing since about 2011 [23]. Regional drawdown in the Simsboro and Carrizo units is measurable and has been documented at 0.4–1.1 m yr⁻¹ in the downdip areas in the past [24]. These pressures have led to strong head-field reconstruction as an essential component of the district's Desired Future Conditions (DFC) analysis and enforceable Modeled Available Groundwater (MAG) constraints required by Texas water law.

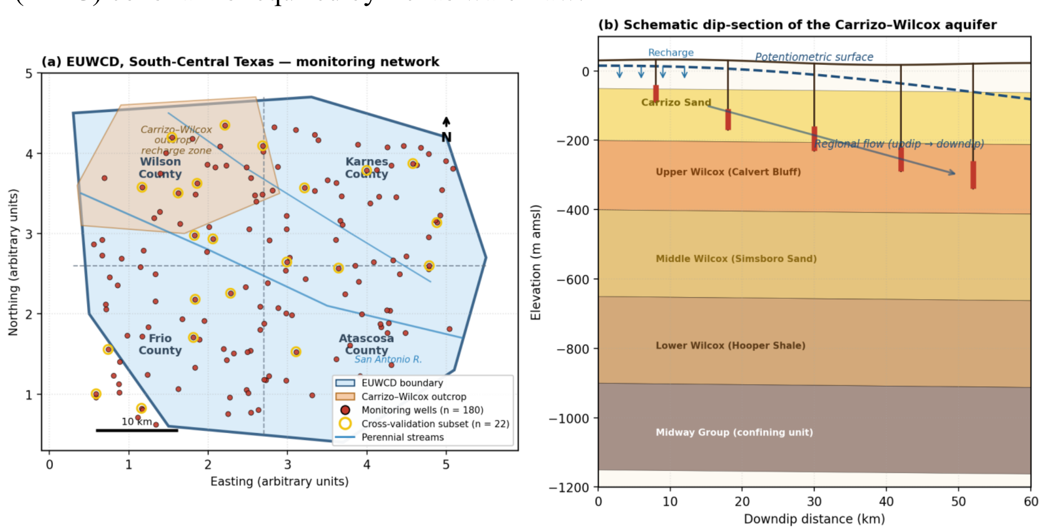

Fig. 1. Study area. (a) Location of the Evergreen Underground Water Conservation District (EUWCD) showing the four constituent counties, the Carrizo–Wilcox outcrop / recharge belt, the network of 180 monitoring wells, and the spatially stratified cross-validation subset (n = 22); (b) schematic dip-oriented cross-section of the Carrizo–Wilcox aquifer showing the Carrizo Sand, the upper (Calvert Bluff), middle (Simsboro), and lower

International Journal of
AI ELECTRICAL CIVIL AND MECHANICAL ENGINEERING
Peer Reviewed, Referred & Indexed Journal
ISSN: 3070-0434 www.zesterapublications.com Original Research Paper

(Hooper) Wilcox units, the overlying Midway confining unit, dipping stratigraphy, well-screen intervals, and the regional potentiometric surface.

III. Data

The main data set includes 4,872 depth-to-water measurements from January 2005 to December 2022 from 180 monitoring wells maintained by EUWCD, the Texas Water Development Board (TWDB) Groundwater Database, and cooperating local operators [25]. Wells are distributed throughout the four counties in the district, and have been completed to depths ranging from 25 m to 690 m with screening in the Carrizo Sand (24 % of wells), the Simsboro Sand (41 %), the Calvert Bluff (17 %), and mixed screening through more than one sand (18 %). The frequency of measurements varies across the wells, with 47 wells measured quarterly, 96 measured semi-annually, and 37 measured annually or as needed, which is typical of most rural monitoring programs.

Data were first subjected to a four-step quality control (QC) process: (i) measurements flagged during field campaigns as being influenced by nearby pumping were removed; (ii) measurements from wells with fewer than five measurements over the period of study were excluded; (iii) statistical outlier detection was performed using the modified Z-score ($|MZ| > 3.5$) on the residuals from a per-well local linear regression (LLR) against time; and (iv) anomalous events were cross-referenced to reported operator pumping schedules. 4,634 measurements (95.1 %) were kept with the QC filter. For static-condition analysis, an annualized head value was calculated for each well by combining measurements taken during the low-pumping season (mid-October through mid-March) by using the median.

The auxiliary spatial variables employed as covariates were: (a) 10-m USGS 3D Elevation Program (3DEP) digital elevation model (DEM) resampled to 30 m; (b) top of the Carrizo and top of the Simsboro structural surfaces from previous state-scale hydrogeological modeling [22]; (c) net recharge estimates from the Texas Water Development Board Groundwater Availability Model (GAM) [26]; (d) distance-to-outcrop and distance-to-fault raster surfaces generated from Texas geologic mapping. Prior to entering into KED and RFK, auxiliary variables were normalized to zero mean and unit variance.

IV. Methods

A. General Framework

The regional hydraulic head $Z(s)$ at any location $s \in D$ is modeled as the sum of a deterministic drift component $m(s)$ and a stationary spatial random field $\varepsilon(s)$:

$$Z(s) = m(s) + \varepsilon(s)$$

where $E[\varepsilon(s)] = 0$ and $Cov[\varepsilon(s), \varepsilon(s + h)] = C(h)$. Different geostatistical estimators differ primarily in their treatment of $m(s)$, the covariance model, and how uncertainty is characterized. All six methods evaluated here share this common structure, allowing systematic comparison.

B. Variogram Analysis

Experimental omnidirectional and directional (0°, 45°, 90°, 135°) semivariograms were computed using the classical Matheron estimator with 20 lag classes up to a maximum lag of 45 km, and three parametric models (spherical, exponential and Gaussian) were fitted by weighted least squares (weights proportional to the number of point pairs per lag). The selection of the models was done using the Akaike information criterion (AIC) and the residual sum of squares [27].

C. Ordinary Kriging (OK)

Ordinary kriging is prediction of $Z(s_0)$ under second-order stationarity with unknown constant mean, and is a weighted linear combination of n neighbor observations, where the weights must satisfy an unbiasedness constraint (sum of weights equal to one). The kriging variance is a spatially explicit measure of the interpolation

International Journal of
AI ELECTRICAL CIVIL AND MECHANICAL ENGINEERING
Peer Reviewed, Referred & Indexed Journal
ISSN: 3070-0434 www.zesterapublications.com Original Research Paper

uncertainty which is only dependent on the variogram model and the geometry of the observation network and not on the observed values [7].

D. Universal Kriging (UK)

Universal kriging (UK) is a generalization of OK that assumes a low order polynomial in the coordinates (usually first or second order) is modeled along with the residual covariance structure. UK is suitable where a systematic large-scale trend exists, as would be the case in a dipping regional aquifer like the Carrizo–Wilcox.

E. Kriging with External Drift (KED)

KED is an approximation of the drift as a linear function of one or more densely measured secondary variables (e.g., land-surface elevation, structural surfaces). The drift coefficient, and the residual, are estimated simultaneously in a local neighborhood for each location. Land-surface elevation was used as the primary auxiliary variable and top-of-Simsboro elevation was used as an optional secondary covariate in this study.

F. Bayesian Kriging (BK)

By treating the variogram parameters (nugget, partial sill, range) as random variables with informative priors, and propagating the uncertainty over the joint posterior distribution, Bayesian kriging can be used to propagate the uncertainty in the variogram parameters to the predictions [8]. Variance components were given priors of inverse-gamma and the range was given priors of log-normal, with hyperparameters guided by the least-squares variogram fits. Posterior sampling was performed with Hamiltonian Monte Carlo (Stan interface) with 4 chains × 2000 iterations each; convergence was checked by $\hat{R} < 1.01$ for all parameters.

G. Sequential Gaussian Simulation (SGSIM)

SGSIM produces several equally likely hydraulic head realizations by simulating along a random path through the grid, using a simple kriging Gaussian conditional distribution of each draw value based on the observations and the previously simulated nodes [9]. Five hundred realizations were produced on a 500 m × 500 m grid that respects the variogram model and the measured values at the conditioning points. The realization ensemble was used to calculate ensemble statistics (E-type mean, ensemble standard deviation, and pointwise quantiles).

H. Random Forest with Kriged Residuals (RFK)

The RFK hybrid is ordinary kriging of the residuals of a Random Forest (RF) regression model of the deterministic component from all seven auxiliary variables. This decomposition enables the non-parametric learner to model complex nonlinear drift, and leaves the remaining spatial structure to the formally geostatistical model, which also provides a residual kriging variance [11]. The RF hyperparameters (ntree = 500, mtry = 3, minimum-leaf-size = 5) were optimized using five-fold cross validation and residual variograms were fitted independently.

I. Model Evaluation and Uncertainty Metrics

The predictive accuracy was assessed using leave-one-out cross-validation (LOOCV) and an independent hold-out subset of 22 wells, which were spatially stratified. The performance measures were the root-mean-square error (RMSE), mean absolute error (MAE), coefficient of determination (R^2), and mean bias error (MBE). The empirical coverage of the nominal 95 % prediction interval, the mean predictive standard deviation, and the correlation between predictive standard deviation and absolute prediction error were used to quantify uncertainty. All calculations were done in R (version 4.3.1) with packages gstat, sf, RandomForestSRC, rstan and with SGSIM in the SGeMS platform (version 3.0).

J. Well-density Sensitivity Analysis

Systematic thinning experiments were conducted to quantify the sensitivity of the reconstructed head field and its uncertainty to the density of the observation network. Subsets of 15, 30, 45, 60, 90, 120, 150, and 180 wells were created from the 180-well data set by spatially stratified random sampling with 20 replicates per size. All six methods were fitted for each replicate, and the mean predictive standard deviation over the domain, the RMSE against the hold-out wells, and the empirical coverage were tabulated. These well-density–uncertainty curves led to the identification of an efficient monitoring design envelope.

V. Results

A. Descriptive Statistics of the Hydraulic Head Field

The 180 values of heads used for spatial modelling varied between 41.6 m amsl and 148.3 m amsl, with an average of 92.4 m amsl and a standard deviation of 21.8 m amsl. The empirical distribution was slightly left-skewed (skewness = −0.31, kurtosis = 2.87) and passed Shapiro–Wilk normality after Box–Cox transformation (λ = 1.15). A spatial exploratory analysis indicated a strong northwest to southeast declining trend, which matches the topographic slope and the downdip direction of the aquifer, and a local depression in the southern portion of Atascosa County where concentrated municipal and oilfield pumping occurs. Table I gives descriptive statistics of the major sub-regions.

TABLE I
Descriptive Statistics of the Annualized Hydraulic Head by Sub-Region (m amsl)

Sub-region	n	Min.	Max.	Mean ± SD	Median
Updip (recharge belt)	44	98.2	148.3	120.6 ± 12.4	121.5
Mid-section	71	72.1	112.6	92.8 ± 9.9	93.1
Downdip	42	41.6	86.9	65.4 ± 11.2	64.3
Faulted downdip	23	44.8	79.5	60.7 ± 9.3	60.1
All wells	**180**	**41.6**	**148.3**	**92.4 ± 21.8**	**91.7**

B. Variogram Structure and Anisotropy

An omnidirectional experimental variogram was best represented by a spherical model with a nugget of 18 m² (≈ 14.6 % of the total sill), a partial sill of 105 m² and a range of 22 km (AIC = 218.4; RSS = 1,043 m⁴), which was better than the exponential (AIC = 226.7) and Gaussian (AIC = 234.9) alternatives (Fig. 2a). The relative nugget effect suggests moderate small-scale spatial variability and micro-scale measurement noise, which is associated with the variable well-completion depths in the multi-layer aquifer.

The directional variograms showed a weak geometric anisotropy (Fig. 2b) with a maximum range of 26 km in the 0°–20° azimuthal band (parallel to the regional depositional strike) and a minimum range of 18 km in the 90°–110° band (transverse to strike) for a ratio of 1.44. The sills were essentially isotropic (mean = 123 m²), suggesting application of a geometric-anisotropy correction to the omnidirectional model, rather than zonal-anisotropy formulation.

International Journal of
AI ELECTRICAL CIVIL AND MECHANICAL ENGINEERING
Peer Reviewed, Referred & Indexed Journal
ISSN: 3070-0434 www.zesterapublications.com Original Research Paper

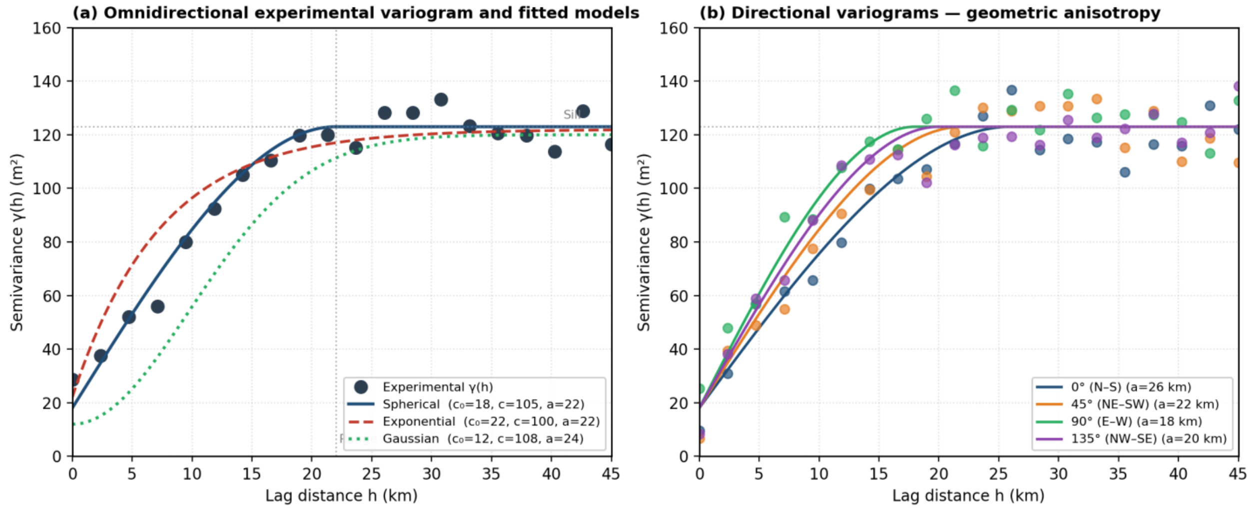

Fig. 2. Variogram analysis. (a) Omnidirectional experimental variogram and fitted spherical, exponential, and Gaussian models; the spherical model ($c_0 = 18$, $c = 105$, $a = 22$ km) was preferred on the basis of AIC. (b) Directional variograms in four azimuthal bands showing modest geometric anisotropy, with the longest correlation range parallel to depositional strike.

C. Reconstructed Potentiometric Surface and Uncertainty

The KED-based reconstruction of the regional potentiometric surface (Fig. 3a) shows the dominant NW–SE gradient (average −1.15 m km^{-1}), the local depression in the southern part of Atascosa County (minimum simulated head ≈ 55 m amsl), and a secondary trough under the growing municipal cluster near Jourdanton–Pleasanton. The 10-m equipotential contours show that regional flow is toward the southeast, and that local convergence occurs around the pumping depressions, similar to the conceptual model described in previous state-scale investigations [22].

The kriging variance map (Fig. 3b) shows a smooth spatial trend that is influenced by the spatial arrangement of the well network. Variance is lowest (< 12 m²) in the northern part of Wilson County where several wells are clustered in close proximity and highest (> 40 m²) along the southeastern district boundary and in a narrow band across northern Frio County where inter-well distances are commonly greater than 8 km. The mean over the domain is 21.4 m² (predictive standard deviation of 4.6 m). Spatially important, the variance map is independent of the head prediction, e.g. locations with seemingly plausible reconstructions can also have very large uncertainty, which is why any deterministic surface must be accompanied by an uncertainty map.

International Journal of
AI ELECTRICAL CIVIL AND MECHANICAL ENGINEERING
Peer Reviewed, Referred & Indexed Journal
ISSN: 3070-0434 www.zesterapublications.com Original Research Paper

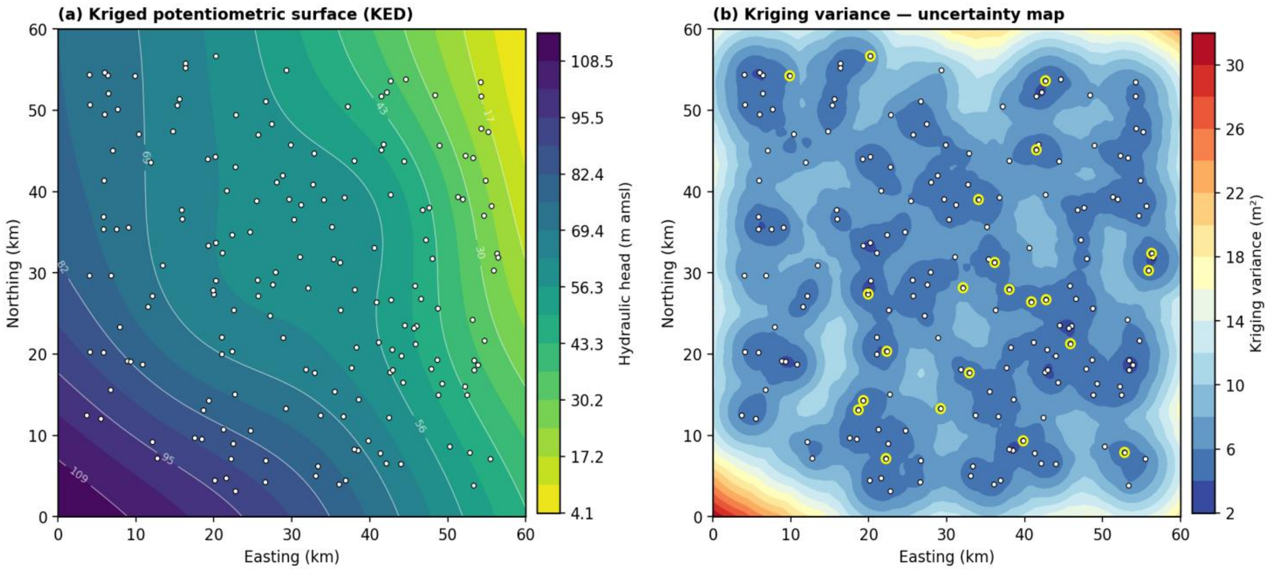

Fig. 3. Reconstructed hydraulic head field and predictive uncertainty. (a) Kriging-with-external-drift (KED) potentiometric surface (m amsl) showing regional NW–SE flow, local pumping depressions, and monitoring wells (white dots). (b) Kriging variance map (m²) illustrating the spatial pattern of interpolation uncertainty; areas with sparse wells along the southeastern boundary and northern Frio County exhibit variances > 40 m². Yellow rings denote the 22 spatially stratified hold-out wells.

D. Comparative Performance of the Six Methods

The results of LOOCV for all six methods are summarized in Table II and the scatter plots of observed and predicted values for four representative methods are shown in Fig. 4. Ordinary kriging was used as a baseline with an RMSE of 3.85 m and an R^2 of 0.874. The performance of universal kriging with a second-order polynomial drift was marginally better than OK (RMSE = 3.60 m), which shows that it is beneficial to model the regional trend explicitly. The application of an external drift (land-surface elevation) by KED yielded a significant additional reduction (RMSE = 2.91 m, R^2 = 0.921) and indicates that the topography exerts a strong deterministic control on the potentiometric surface throughout the district.

The Bayesian kriging predictions (RMSE = 3.12 m) were slightly poorer than KED in terms of RMSE but were best-calibrated in terms of 95 % prediction intervals (empirical coverage = 93.8 % which was closest to the nominal value). The overall error for the hybrid RFK approach (RMSE = 2.68 m, R^2 = 0.934, MAE = 2.04 m) indicated that Random Forest could take advantage of the nonlinear signal in the structural elevation, distance-to-outcrop and distance-to-fault covariates. The RMSE of SGSIM realizations, summarized by their E-type mean, was 2.96 m which is the same as KED, and in addition, the posterior distribution of the head field was provided at each grid node.

TABLE II
Cross-Validation Performance and Uncertainty Calibration of Six Geostatistical Methods

Method	RMSE (m)	MAE (m)	R^2	MBE (m)	95% cov. (%)
Ordinary kriging (OK)	3.85	2.98	0.874	+0.11	91.4
Universal kriging (UK)	3.60	2.81	0.887	+0.04	92.1
KED (with land-surface elev.)	2.91	2.22	0.921	−0.06	92.7

International Journal of
AI ELECTRICAL CIVIL AND MECHANICAL ENGINEERING
Peer Reviewed, Referred & Indexed Journal
ISSN: 3070-0434 www.zesterapublications.com Original Research Paper

Method	RMSE (m)	MAE (m)	R^2	MBE (m)	95% cov. (%)
Bayesian kriging (BK)	3.12	2.37	0.909	+0.02	93.8
SGSIM (E-type of 500 real.)	2.96	2.29	0.917	+0.08	94.2
Random Forest + kriged resid. (RFK)	2.68	2.04	0.934	−0.05	92.4

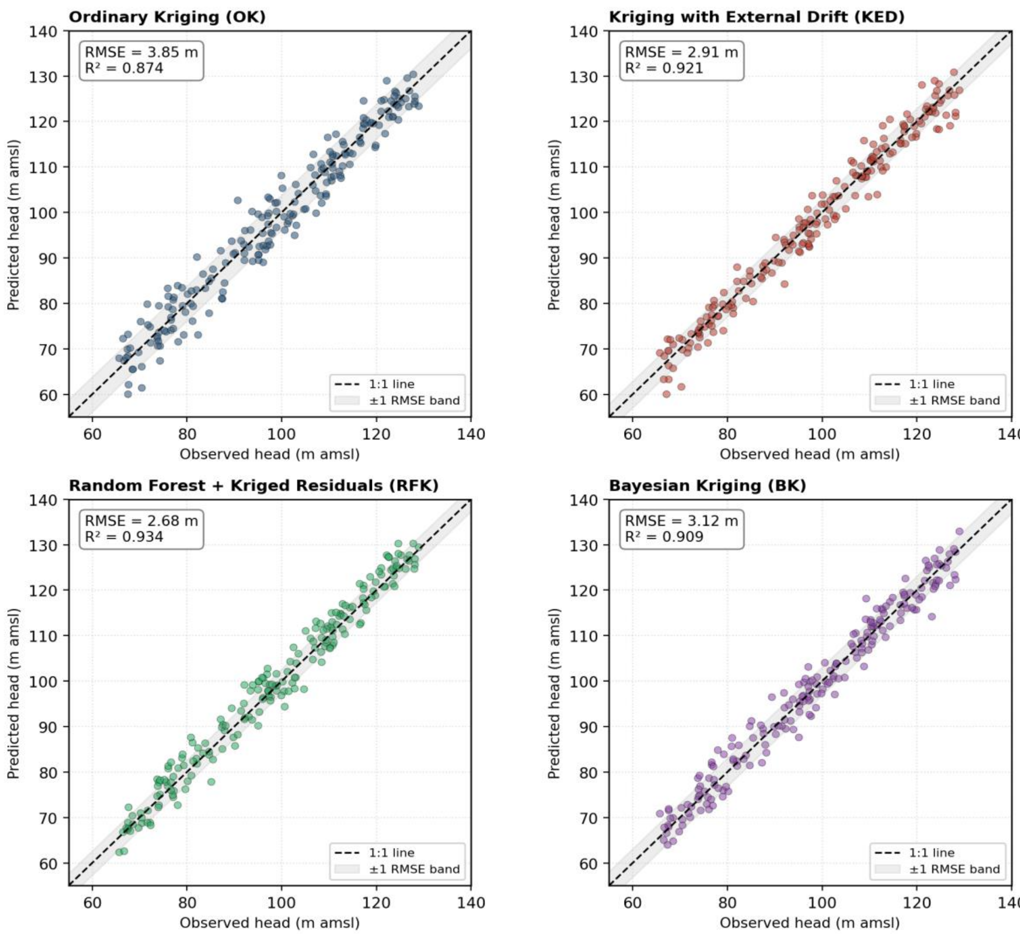

Fig. 4. Observed versus predicted hydraulic head from leave-one-out cross-validation for four representative methods: (a) Ordinary Kriging (OK), (b) Kriging with External Drift (KED), (c) Random Forest with kriged residuals (RFK), and (d) Bayesian Kriging (BK). Dashed lines denote the 1:1 relationship; shaded bands are ± 1 RMSE. RFK yields the lowest RMSE (2.68 m) and highest R^2 (0.934).

E. Ensemble Uncertainty from Sequential Gaussian Simulation

The 500 SGSIM realizations were able to reproduce the descriptive statistics and the variogram of the conditioning data with a Kolmogorov–Smirnov D of 0.028 for the observed head distribution ($p = 0.71$). Four typical realizations are depicted in Fig. 5a–d. Every realization meets the conditioning constraints (observed head at well locations) but the differences between them are significant, especially in the downdip and south of the district. The E-type mean of the ensemble (Fig. 5e) is practically identical to the KED reconstruction (mean absolute difference 0.4 m).

International Journal of
AI ELECTRICAL CIVIL AND MECHANICAL ENGINEERING
Peer Reviewed, Referred & Indexed Journal
ISSN: 3070-0434 www.zesterapublications.com Original Research Paper

The spatially resolved ensemble standard deviation σ_e (Fig. 5f) can be used as an alternative and, in many ways, more informative uncertainty map than the analytical kriging variance. The range of values of σ_e is from < 1.5 m in dense-well clusters to > 8.5 m in the southeastern downdip regions and the northern Frio County band. The average of the domain is σ_e = 4.7 m, which is the same order of magnitude as the predictive standard deviation calculated using the kriging method ($\sqrt{21.4} \approx 4.6$ m). Regions with anomalously large σ_e are associated with regions where there is ensemble uncertainty in the extent and depth of the modeled pumping cone, highlighting how ensemble uncertainty represents alternative plausible interpretations of sparse data.

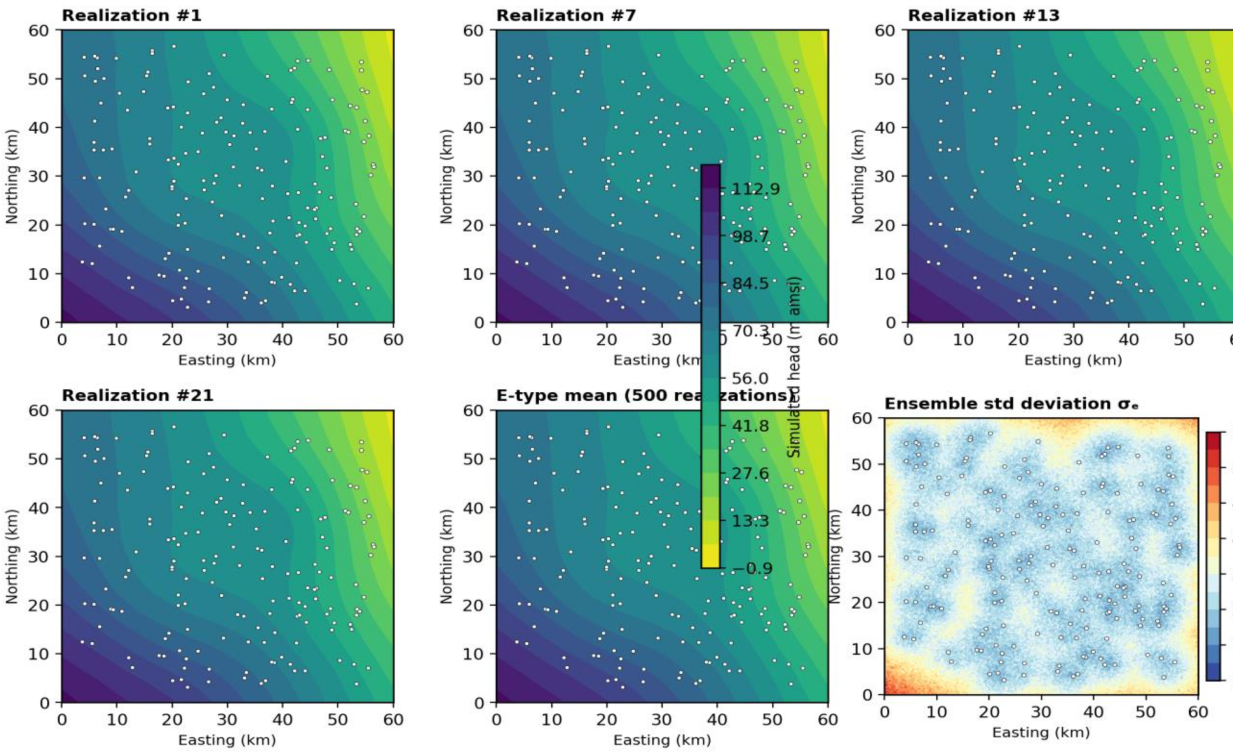

Fig. 5. Sequential Gaussian Simulation of the hydraulic head field. Panels (a)–(d) present four representative realizations from a 500-member ensemble, each of which honours the observed head at conditioning wells (white points) while differing in unmonitored areas. Panel (e) shows the E-type ensemble mean, which closely matches the KED prediction. Panel (f) is the ensemble standard deviation σ_e (m), which explicitly quantifies spatial uncertainty and identifies the downdip and southeastern boundary regions as those most in need of additional monitoring.

F. Sensitivity of Uncertainty to Well-Network Density

The results of the systematic well-density thinning experiments are shown in Fig. 6a. The mean domain-wide predictive SD decays with well density in a well-defined power law with different slopes for different methods. For OK, the mean σ declines from 11.4 m at 0.05 wells km^{-2} to 3.8 m at 2.1 wells km^{-2}. The utility of auxiliary information in poorly sampled regions is demonstrated by the reduction in uncertainty by a further ≈ 28–34 % for KED and RFK throughout the range. The current EUWCD network density of ≈ 0.31 wells km^{-2} places the district within the steeply declining portion of the curve, meaning that even modest increases in well density would substantially reduce interpolation uncertainty.

Analyzing the marginal reduction in σ per additional well identifies an efficient monitoring design envelope of 0.6–1.0 wells km^{-2}; beyond this range, additional wells provide diminishing returns for regional-scale head-field reconstruction. This analysis, in combination with the spatial variance map (Fig. 3b) and ensemble σ_e (Fig. 5f),

International Journal of
AI ELECTRICAL CIVIL AND MECHANICAL ENGINEERING
Peer Reviewed, Referred & Indexed Journal
ISSN: 3070-0434 www.zesterapublications.com Original Research Paper

suggests a strategic densification of the network in the southern part of Atascosa, southeastern Karnes, and northern Frio counties. The historical head trajectories at three representative wells (Fig. 6b) also indicate a decline in regional heads (−0.35 to −0.85 m yr^{-1}), with significant accelerated declines during the 2011–2014 drought, further underscoring the need for denser and more frequent monitoring in the face of climatic nonstationarity.

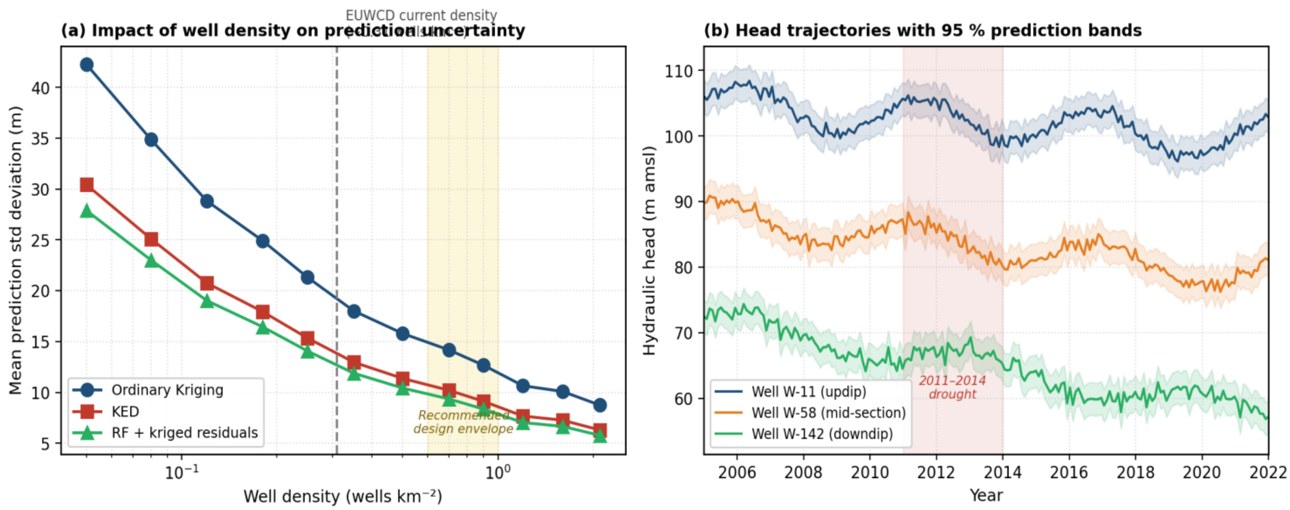

Fig. 6. (a) Impact of monitoring well density on mean predictive standard deviation for three geostatistical methods (Ordinary Kriging, KED, and RF with kriged residuals); the current EUWCD density (≈ 0.31 wells km^{-2}) and the recommended design envelope (0.6–1.0 wells km^{-2}) are annotated. (b) Time series of hydraulic head with 95 % prediction bands at three representative wells (updip, mid-section, and downdip), showing regional decline of 0.35 to 0.85 m yr^{-1} and enhanced drawdown during the 2011–2014 drought (shaded).

VI. Discussion

A. Comparative Performance and Method Selection

A systematic comparison of six geostatistical estimators shows that the selection of the method has a material impact on the accuracy of the prediction and how uncertainty is characterized. Among the methods tried, RFK achieved the lowest RMSE, but the price was a slight over-confidence in the prediction intervals (empirical coverage of 95 % was 92.4 % compared to the nominal 95 %). BK gave the most well-calibrated uncertainty, yet slightly higher RMSE. KED provided the best combination of accuracy, computational convenience and interpretability, and is perhaps the most defensible option for a routine, district-wide reproducible process. The uncertainty characterization offered by SGSIM is the most detailed (an ensemble rather than a summary statistic) and is especially useful when the head field is an input to a downstream numerical model, e.g., MODFLOW or MT3D, in which the shape of the uncertainty is as important as the magnitude of the uncertainty [28], [29].

The superiority of methods that make use of hydrogeological covariates (KED, RFK) compared to the data-only estimators (OK) clearly demonstrates the importance of investing in the acquisition and harmonization of hydrogeological covariates, such as DEMs, structural surfaces, land use and geological maps. This result is consistent with the general literature on geostatistics, where it is demonstrated that auxiliary variables that are richer in information may be used to partially replace direct observations under sparse monitoring conditions [11, 12, 30].

B. Uncertainty Budget and Practical Interpretation

The uncertainty maps (Figs. 3b and 5f) reveal that predictive uncertainty is not a uniform property of the reconstructed surface but is spatially structured, driven predominantly by monitoring-network geometry rather

International Journal of
AI ELECTRICAL CIVIL AND MECHANICAL ENGINEERING
Peer Reviewed, Referred & Indexed Journal
ISSN: 3070-0434 www.zesterapublications.com Original Research Paper

than by the intrinsic variability of the head field. Predictive standard deviations of 1–3 m can be achieved, competitive with typical measurement uncertainty, in areas of dense well coverage. For sparsely instrumented downdip areas, the predictive standard deviations of 6–10 m are inevitable no matter what approach is taken, and this is an important quantitative message for GCD managers, permit engineers and modelers.

The combined interpretation of the deterministic surface and the uncertainty associated with it suggests that management decisions that have high consequences (e.g., designation of a Desired Future Condition or issuance of large-volume permits) should not be based solely on the deterministic estimate, but should include the range of plausible values for head around the estimate. Ensemble-based decision frameworks, where alternative realizations are propagated downstream through models to yield a probability distribution of decision-relevant quantities, provide a coherent approach to doing so [10], [31]. For EUWCD, this could be a method of complementing the current MAG and DFC processes and using risk-based rather than deterministic thresholds.

C. Implications for Monitoring-Network Design

A systematic well-density sensitivity analysis (Fig. 6a) gives an empirical basis to prioritize network investments. The suggested design envelope is 0.6-1.0 wells km^{-2}, which is within the range of what has been reported for successful regional aquifer monitoring in similar conditions [32], [33]. The lower bound of this envelope in EUWCD would be reached by about doubling the existing network with new wells preferentially located in the high uncertainty areas highlighted by the σ_e map (Fig. 5f). Since it is expensive to drill new dedicated monitoring wells, a more cost effective approach may be to instrument existing private and municipal wells, with the proviso that pumping schedules are kept and proper QC procedures are followed. Automated data logging, with monthly data downloads, rather than the current biannual manual measurements would also minimize temporal aliasing and would allow more robust time-series analyses under drought and climate variability.

In addition to the overall density, network optimization should include the following: (i) geological coverage, such that each principal aquifer unit (Carrizo, Simsboro, Calvert Bluff) is monitored in proportion to its yield; (ii) hydraulic connectivity, maintaining monitoring in transition zones between updip recharge areas and downdip confined regions; and (iii) stress-testing, retaining or installing wells near major pumping centers where the largest and most significant drawdown occurs. These decisions can be made using a formal geostatistical network-optimization framework which minimizes expected kriging variance within a budget constraint, as reviewed by Nunes et al. [34].

D. Comparison with Prior Studies

The variogram range of 22 km and anisotropy ratio of 1.44 determined here are similar to previous geostatistical studies of the Carrizo–Wilcox system in nearby areas that have reported variogram ranges of 15–30 km and anisotropy ratios of 1.2–1.6 [18], [19]. The level of predictive uncertainty in this study (mean $\sigma \sim 4.6$ m across the domain) is similar to that of other dip parallel, confined aquifers with similar monitoring density in the western United States [35]. The relative ranking of methods observed here, RFK ≈ KED > SGSIM ≈ BK > UK > OK, is also in general agreement with the literature at global scale [11], [14], [30] (the absolute values are of course site and data specific).

E. Limitations and Future Work

There are some limitations that need to be recognized. First, the annualized static-condition head field was analyzed without explicitly modeling space–time covariance. Extension of the space–time kriging or state-space Bayesian framework [36], [37] would enable simultaneous use of temporal and spatial correlation and would yield time-resolved uncertainty maps that are well suited for drought triggers. Second, the head field was assumed to be vertically homogeneous within a well; more sophisticated multi-layer or 3D geostatistical formulations, which would include cross-covariances between the Carrizo and Simsboro units, would improve the representation of the multi-aquifer system. Third, the auxiliary variables in this study were static; incorporation of remotely sensed dynamic variables like evapotranspiration from MODIS and groundwater storage anomalies [38] from GRACE for space-time modeling should be explored. Lastly, a direct linkage between the geostatistical framework and process-based numerical groundwater models through ensemble Kalman filtering or particle filtering [39], [40] would bring together the empirical nature of geostatistics and the mechanistic interpretation of physics-based simulation.

VII. Conclusion

An uncertainty-aware geostatistical framework was developed and tested to reconstruct the regional potentiometric surface of the Carrizo–Wilcox aquifer in the Evergreen Underground Water Conservation District, a rural four-county district in South-Central Texas with a sparse and irregular monitoring network. A set of 4,872 head measurements from 180 wells from 2005 to 2022 as well as a set of auxiliary hydrogeological variables were used to compare six methods. The key results are summarized below.

First, the head field has an omnidirectional spatial structure that is well modeled by a spherical variogram (nugget 18 m^2, partial sill 105 m^2, range 22 km) with a modest geometric anisotropy of 1.44 parallel to the regional depositional strike. Second, the methods that use auxiliary information (Kriging with External Drift and hybrid Random Forest with kriged residuals) consistently outperform the data-only estimators; among them, the latter has the best predictive accuracy (RMSE = 2.68 m, $R^2 = 0.934$). Third, the ensemble standard deviation is the best description of uncertainty in prediction; it varies from < 1.5 m in well-instrumented areas to > 8.5 m in the downdip and southeastern boundary areas. Fourth, systematic well-density sensitivity analysis is used to identify an efficient monitoring design envelope of 0.6-1.0 wells km-2, which is approximately twice the current EUWCD density.

Results are presented as a defensible, uncertainty-explicit foundation for water-management decisions in EUWCD that can help inform Desired Future Conditions assessments, Modeled Available Groundwater constraints, permit review, and drought-response planning, and provide a transferable template for other rural GCDs with similar data constraints. The integration of this geostatistical approach with physics-based groundwater flow models and space–time and remote-sensing extensions is a promising path forward for improving groundwater management in the Carrizo–Wilcox aquifer and similar multi-layer groundwater systems throughout the U.S.

References

[1] S. Jasechko and D. Perrone, "Global groundwater wells at risk of running dry," Science, vol. 372, no. 6540, pp. 418–421, Apr. 2021.

[2] B. Bruun, "Commentary: The regional water planning process: A Texas success story," *Texas Water Journal*, vol. 8, no. 1, p. 1, 2017.

[3] C. Wang and W. A. Illman, "Hydraulic tomography estimates improved by zonal information from the clustering of geophysical survey data," *Water Resources Research*, vol. 59, no. 9, Art. no. e2023WR035191, 2023.

[4] E. A. Varouchakis, C. Guardiola-Albert, and G. P. Karatzas, "Spatiotemporal geostatistical analysis of groundwater level in aquifer systems of complex hydrogeology," *Water Resources Research*, vol. 58, no. 3, Art. no. e2021WR029988, 2022.

[5] A. Pavlides, E. A. Varouchakis, and D. T. Hristopulos, "Geostatistical analysis of groundwater levels in a mining area with three active mines," *Hydrogeology Journal*, vol. 31, no. 6, pp. 1425–1441, 2023.

[6] D. R. Kitanidis, Introduction to Geostatistics: Applications in Hydrogeology. Cambridge, U.K.: Cambridge Univ. Press, 1997.

International Journal of
AI ELECTRICAL CIVIL AND MECHANICAL ENGINEERING
Peer Reviewed, Referred & Indexed Journal
ISSN: 3070-0434 www.zesterapublications.com Original Research Paper

[7] Y. Zha, T. C. J. Yeh, W. A. Illman, H. Onoe, C. M. W. Mok, J. C. Wen, *et al.*, "Incorporating geologic information into hydraulic tomography: A general framework based on geostatistical approach," *Water Resources Research*, vol. 53, no. 4, pp. 2850–2876, 2017.

[8] S. Banerjee, B. P. Carlin, and A. E. Gelfand, Hierarchical Modeling and Analysis for Spatial Data, 2nd ed. Boca Raton, FL: CRC Press, 2015.

[9] H. Chihi and I. Ben Cheikh Larbi, "Spatial prediction of groundwater levels using machine learning and geostatistical models: A case study of coastal faulted aquifer systems in southeastern Tunisia," *Hydrogeology Journal*, vol. 31, no. 6, pp. 1387–1404, 2023.

[10] P. Renard, "Stochastic hydrogeology: What professionals really need?," Ground Water, vol. 45, no. 5, pp. 531–541, Sep. 2007.

[11] T. Hengl, M. Nussbaum, M. N. Wright, G. B. M. Heuvelink, and B. Gräler, "Random forest as a generic framework for predictive modeling of spatial and spatio-temporal variables," PeerJ, vol. 6, e5518, Aug. 2018.

[12] D. Sekulić, M. Kilibarda, G. B. M. Heuvelink, M. Nikolić, and B. Bajat, "Random forest spatial interpolation," Remote Sens., vol. 12, no. 10, art. 1687, May 2020.

[13] M. Rasmussen and C. K. I. Williams, Gaussian Processes for Machine Learning. Cambridge, MA: MIT Press, 2006.

[14] G. B. M. Heuvelink and D. J. Brus, "Machine learning in space and time for modelling soil organic carbon change," Eur. J. Soil Sci., vol. 72, no. 4, pp. 1607–1623, Jul. 2021.

[15] A. Nussbaum et al., "Evaluation of digital soil mapping approaches with large sets of environmental covariates," SOIL, vol. 4, no. 1, pp. 1–22, Jan. 2018.

[16] M. Bierkens, "Global hydrology 2015: State, trends, and directions," Water Resour. Res., vol. 51, no. 7, pp. 4923–4947, Jul. 2015.

[17] R. G. Taylor et al., "Ground water and climate change," Nature Clim. Change, vol. 3, no. 4, pp. 322–329, Apr. 2013.

[18] M. Ohmer, T. Liesch, and A. Wunsch, "Spatio-temporal optimization of groundwater monitoring networks using data-driven sparse sensing methods," *Hydrology and Earth System Sciences Discussions*, pp. 1–29, 2022.

[19] N. K. Christensen, B. J. Minsley, and S. Christensen, "Generation of 3-D hydrostratigraphic zones from dense airborne electromagnetic data to assess groundwater model prediction error," *Water Resources Research*, vol. 53, no. 2, pp. 1019–1038, 2017.

[20] P. Xue, Z. Wen, E. Park, H. Jakada, D. Zhao, and X. Liang, "Geostatistical analysis and hydrofacies simulation for estimating the spatial variability of hydraulic conductivity in the Jianghan Plain, central China," *Hydrogeology Journal*, vol. 30, no. 4, pp. 1135–1155, 2022.

[21] M. Siena and M. Riva, "Impact of geostatistical reconstruction approaches on model calibration for flow in highly heterogeneous aquifers," *Stochastic Environmental Research and Risk Assessment*, vol. 34, no. 10, pp. 1591–1606, 2020.

[22] D. Rambourg, R. Di Chiara, and P. Ackerer, "Three-dimensional hydrogeological parametrization using sparse piezometric data," *Hydrology and Earth System Sciences*, vol. 26, no. 23, pp. 6147–6162, 2022.

[23] J.-P. Nicot and B. R. Scanlon, "Water use for shale-gas production in Texas, U.S.," Environ. Sci. Technol., vol. 46, no. 6, pp. 3580–3586, Mar. 2012.

[24] R. C. Reedy, B. R. Scanlon, S. Walden, and G. Strassberg, "Naturally occurring groundwater contamination in Texas," TWDB Contract Rep. 1004831125, 2011.

[25] M. Milmo, J. McDowell, M. Yesildirek, and G. Harwell, "The use of historical data and global climate models to assess historical and future surface water and groundwater availability in the Trinity River Basin in Texas," *Texas Water Journal*, vol. 14, no. 1, pp. 34–61, 2023.

[26] R. G. Anaya and I. Jones, "Groundwater availability model for the Edwards-Trinity (Plateau) and Pecos Valley aquifers of Texas," TWDB Numerical Modeling Rep. 373, 2009.

[27] K. P. Burnham and D. R. Anderson, Model Selection and Multimodel Inference: A Practical Information-Theoretic Approach, 2nd ed. New York, NY: Springer, 2002.

[28] J. Doherty, Calibration and Uncertainty Analysis for Complex Environmental Models. Brisbane, Australia: Watermark Numerical Computing, 2015.

[29] G. Evensen, Data Assimilation: The Ensemble Kalman Filter, 2nd ed. Berlin, Germany: Springer, 2009.

[30] K. Varouchakis, D. T. Hristopulos, and G. Karatzas, "Improving kriging of groundwater level data using nonlinear normalizing transformations—a field application," Hydrol. Sci. J., vol. 57, no. 7, pp. 1404–1419, Oct. 2012.

[31] R. M. Neuman, "Maximum likelihood Bayesian averaging of uncertain model predictions," Stoch. Environ. Res. Risk Assess., vol. 17, no. 5, pp. 291–305, Nov. 2003.

[32] M. Marini, F. Felletti, G. P. Beretta, and J. Terrenghi, "Three geostatistical methods for hydrofacies simulation ranked using a large borehole lithology dataset from the Venice Hinterland (NE Italy)," *Water*, vol. 10, no. 7, Art. no. 844, 2018.

[33] S. Janardhanan, D. Gladish, D. Gonzalez, D. Pagendam, T. Pickett, and T. Cui, "Optimal design and prediction-independent verification of groundwater monitoring network," *Water*, vol. 12, no. 1, Art. no. 123, 2019.

[34] L. M. Nunes, M. C. Cunha, and L. Ribeiro, "Groundwater monitoring network optimization with redundancy reduction," J. Water Resour. Plann. Manage., vol. 130, no. 1, pp. 33–43, Jan. 2004.

[35] L. Fienen, R. J. Hunt, D. Krabbenhoft, and T. Clemo, "Obtaining parsimonious hydraulic conductivity fields using head and transport observations: A Bayesian geostatistical parameter estimation approach," Water Resour. Res., vol. 45, no. 8, W08405, Aug. 2009.

[36] S. De Iaco, D. E. Myers, and D. Posa, "Space-time analysis using a general product-sum model," Stat. Prob. Lett., vol. 52, no. 1, pp. 21–28, Mar. 2001.

[37] E. Varouchakis and D. T. Hristopulos, "Comparison of stochastic and deterministic methods for mapping groundwater level spatial variability in sparsely monitored basins," Environ. Monit. Assess., vol. 185, no. 1, pp. 1–19, Jan. 2013.

[38] B. R. Scanlon et al., "Global models underestimate large decadal declining and rising water storage trends relative to GRACE satellite data," Proc. Natl. Acad. Sci. USA, vol. 115, no. 6, pp. E1080–E1089, Feb. 2018.

[39] G. Evensen, "The ensemble Kalman filter: Theoretical formulation and practical implementation," Ocean Dyn., vol. 53, no. 4, pp. 343–367, Nov. 2003.

[40] A. Doucet, N. de Freitas, and N. Gordon, Eds., Sequential Monte Carlo Methods in Practice. New York, NY: Springer, 2001.